SOME CONSIDERATIONS ON
UV OPTICS FOR SYNCHROTRON RADIATION[*]

W. R. McKinney

Brookhaven National Laboratory
Upton, New York 11973

August 1978

SOME CONSIDERATIONS ON

UV OPTICS FOR SYNCHROTRON RADIATION*

.

W. R. McKinney

Brookhaven National Laboratory

Upton, New York   11973

Introduction

While synchrotron radiation (SR) has a broad spectrum extend-
ing from the hard x-ray region (tens of keV) throu;h the visible
and infrared regions (a few eV) the main interest is in those wave-
lengths which are not readily available from other sources; that
is those wavelengths shorter than say 2000Å. This region poses
several problems for the optical designer that do not occur in the
visible region of the spectrum.

1. Between about 2Å and 2000Å wavelength, air (oxygen)
    is not transparent, necessitating the evacuation of
    the equipment.

2. As wavelength decreases an optical surface generally
    redirects an increasing fraction of the incident
    light randomly into 2π solid angle rather than the
    direction desired. This "scattering" of the light
    is due to the wavelength of the SR becoming more
    comparable to the size of irregularities of the
    optical surface.

3. The reflectivity of coatings available for surfaces
    begins to decrease below 2000Å. Below 1200Å, where
    aluminum overcoated with MgF_2 to prevent oxidation

and enhance reflectivity begins to deteriorate, there are no good normal incidence reflectors. (R ≥ 80%)

4. Below ≈ 1100Å, the cutoff wavelength of LiF, there are no materials suitable for refractive surfaces or rigid windows.

Problem 1 can be overcome with effort and money by various means of construction and vacuum pumps. I will not cover this technology except to say that they all introduce hydrocarbons onto the optical surfaces by one route or another. (0-rings, mechanical pump fluid, diffusion pump fluid, turbine pump fluid, and finger-prints.) These hydrocarbons interact photochemically with the high intensity SR forming a layer of contamination which is often assumed to be polymerized hydrocarbons but which may not be.[1] To my knowledge, definitive work on the nature of contamination has not been done and would be a fruitful line of research. There is the possibility that fluorinated pump fluids, such as Fomblin, may be broken into gaseous products by the SR beam which would then be pumped away and not deposited on the optical surfaces.[2]

Problem 2 needs investigation in the areas of surface characterization, scattering mechanisms and angular and energy dependence. Scattering of the SR by optical surfaces may be the most significant limit to available fluxes at high photon energies.[3]

Items 3 and 4 determine the nature of optics in the UV. Mirrors are, in general, necessary below 2000Å. Although potential lens materials exist down to ~ 1200Å (BaF$_2$, CaF$_2$, LiF$_2$), their indices of refraction vary significantly near their cutoff wavelengths, introducing chromatic aberration. Polishing these materials for high transmission and low scattered light is often difficult; although for special applications where the wavelength region of primary interest is not too great, these materials should not be overlooked.[4]

Below 300Å, where normal incidence reflectivity is very low, the mirror must be used in grazing incidence geometry. At high incidence angles (low grazing angles), an electromagnetic effect occurs which can permit total reflection.

Although there are complications to the following simple picture, a basic understanding of its application to SR should ensue. There exists an angle called the critical angle (measured from the tangent to the mirror, i.e., a grazing angle) defined (approximately) by the following equation:

$$\sin \theta c = \lambda \left(\frac{e^2}{mc^2} \frac{N}{\pi} \right)^{-\frac{1}{2}} \quad N = \text{electrons/unit vol.}$$

2

For a given wavelength, total reflection occurs at all angles smaller than the critical angle. On the other hand, for a fixed angle, all wavelengths longer than a certain one will be reflected with very high reflectance. This forms the basis for what is called the "order sorting" mirror in a synchrotron radiation beam line. The purpose of a beam line, unless all of the SR spectrum is desired, is to throw away all of the SR except the wavelength of interest. The first mirror can be set to absorb heavily all of the wavelengths below a given one, accomplishing about one half of the required job of the beam line in the first reflection. The explanation of the term "order sorting" requires a digression into diffraction gratings. Figure 1 shows schematically the fundamental relation for a diffraction grating.

$$d\sin\theta = \pm n\lambda \quad . \quad n = 0,1,2, \ldots$$

Notice that for a given θ there are an infinite number of λ's which can satisfy the relation. For example, if we were at an angle into which 100Å was diffracted with n (order) = 1, then 50Å with order = 2 would also take the same direction, and 33.33Å with n = 3 would also be there. In practice, we are helped by the fact that the efficiency of the grating often goes down with increasing order. Nevertheless, for some experiments, e.g., photochemical ones where higher energy photons can cause reactions not inducible by the first order wavelength, even 5% higher order contamination can be intolerable. Now that we know something about orders, we can see that if the first mirror is a poor reflector below 50Å, for example, second order interference will not become a problem until 100Å. Given enough money, one could have a beam line for each octave of the spectrum and suffer little second order contamination.

This feature of the first mirror has a disadvantage because most of the power in the SR spectrum is in the short wavelengths. Thus, the order sorting mirror which passes only wavelengths on the long λ side of the critical $\lambda = \lambda_c$ must absorb the major fraction of the unwanted SR. In the case of the storage rings under construction at Brookhaven, this can be many watts of energy, particularly for the 2.5 GeV x-ray ring. With I in amperes, E in GeV and B in kilogauss, the power of the photon beam in kilowatts is

$$P = 2.65 \ E^3 IB \ \text{kw (for a circular ring of}$$
$$\text{constant bending field strength)}[5] \ .$$

Let us assume 10KG, 1 ampere and 0.7 GeV for the UV ring and 2.5 GeV for the large ring. This gives about 9100 watts for the UV ring and 414,000 watts for the x-ray ring. Let's specialize on the UV ring. Assume we will collect 100 milliradians (mr). This could be done by a mirror of 20 cm projected length at 2 meters from the source.

Fig. 1a Order Sorting Mirror
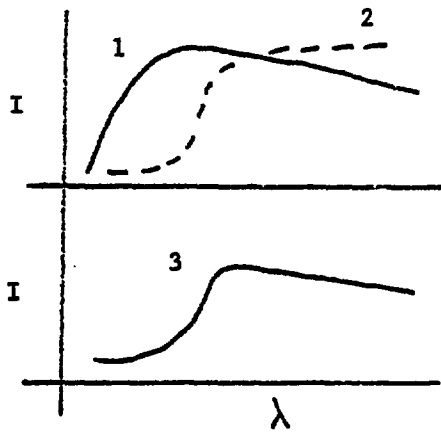
1. SR
2. Mirror reflectivity
3. Transmitted radiation

Fig. 1b Diffraction Grating
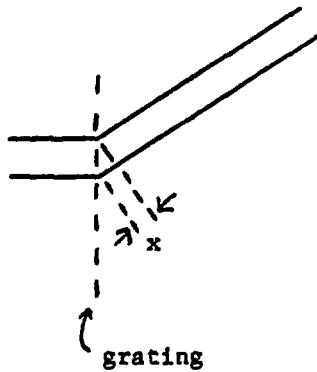
geometry $\Rightarrow$ $x = d\sin\theta$

$x = m\lambda \Rightarrow$ rays in phase
constructive
interference

$$\frac{.001}{2\pi} \times 9100 \text{ watts} = 1.44 \frac{\text{watts}}{\text{mr}}$$

$$0.144 \frac{\text{watts}}{\text{mr}} \times 100 \text{ mr} = 144 \text{ watts} .$$

This is a non-negligible power load which must be considered as a source of changes in mirror figure caused by temperature differences. In addition, the narrow vertical divergence of the hardest photons, ≤ 10 mr, will place for some geometries most of the radiation on a narrow strip (~ 1 mr) down the center of the mirror. The cooling problem becomes severe for the x-ray ring as you can see from the numbers above.

So far, we have realized that we are limited to mirrors and often high incidence (low grazing) angles in order to achieve good reflectivity. Because a major goal in SR beam lines is to place as much radiation at the experimenter's disposal as possible, the radiation must be focused or rendered parallel. If we take the previous case of the collection of 100 mr in the horizontal direction, the divergence of the beam must be altered close to the SR source or the beam will become so wide that one can not afford a mirror big enough to reflect it. Remember, also, that at grazing angles mirrors must be much longer than at normal incidence.

The spherical concave mirror is the first and obvious choice for focusing. It has major advantages in being a simple surface to grind, and is routinely made for many other applications. Its major disadvantage is that it is stigmatic only near normal incidence. That is, it images a point source into a point image only near 0° incidence angle. Figure 2 shows this effect. In part (a), if we place the object at the center of curvature of the sphere, it is easy to see that the image will coincide with the object because rays from the object will be perpendicular to the mirror by definition and the ray will reflect back on itself. If we move away from the center of curvature along the optic axis, the image remains a point and remains on the axis of symmetry. Keep in mind that we are talking about a point and not a finite source.

Part (b) shows the effect of moving the object point off the axis. The primary aberration of spherical mirrors has arisen, astigmatism. (Literally, astigmatism means not spotlike, but its use is reserved to only one class of aberration.) Let's pick a spherical mirror of radius 2000 cm and square shape 5 cm on a side with incidence angle = 10°. If we trace the path of four rays from the object point to the points 1 through 4, and see where they reflect, we find not a point focus but the following. The rays first come together in a vertical line at the horizontal focus; and then, farther from the mirror, they converge into a horizontal line at the vertical focus. Between these two foci, we find what is called
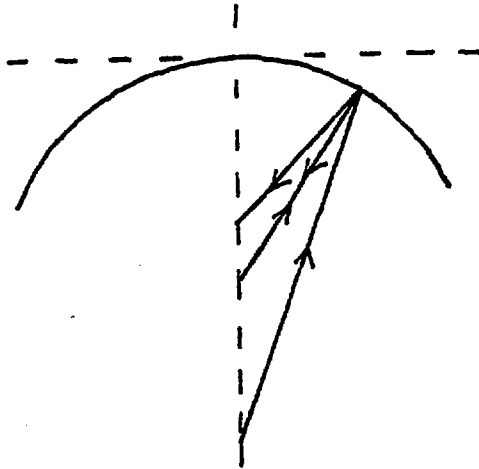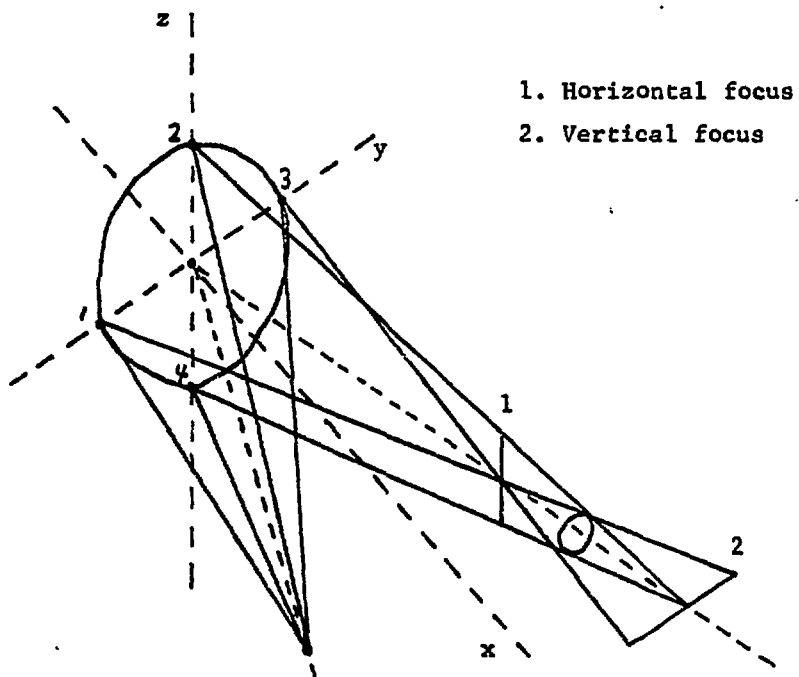
Fig. 2a <u>Spherical Mirror On Axis</u>

Fig 2b <u>Astigmatism of Spherical Mirror</u>

1. Horizontal focus
2. Vertical focus

the "circle of least confusion". For our case, the line of horizontal focus will be 2.97 mm in height, the line of vertical focus 3.11 mm in width, and the diameter of the "spot" in between about 1.50 mm. As the incidence angle grows, the situation gets worse. For our case, holding the object distance of 2000 cm and increasing the incidence angle moves the horizontal and vertical foci farther apart. Indeed, at 60° incidence angle the vertical focus disappears, and the rays do not converge vertically at all. The table in Fig. 2 gives the horizontal and vertical focal lengths and the height of the image at the horizontal focus for several incidence angles. Negative focal lengths indicate that the rays diverge and would cross if their direction were extended behind the mirror. Realize that positive vertical foci could have been retained by moving the object point closer to the mirror.

These focal distances have been obtained by a geometrical ray trace calculation which will be described below. They can also be calculated by the following relations.

$$\frac{1}{0} + \frac{1}{i_H} = \frac{2}{R \cos\phi} \qquad \frac{1}{0} + \frac{1}{i_v} = \frac{2 \cos\phi}{R}$$

ϕ = incidence angle 0 = object distance

i_H = distance to horizontal focus i_v = distance to vertical focus.

This dismal picture of high angle focusing is addressed in the following manner. Let us rewrite the above equations in the form of the on axis equation where $i_H = i_v$, and $f \equiv$ focal length.

$$\frac{1}{0} + \frac{1}{i} = \frac{1}{f}$$

We can then identify

$$\frac{R \cos\phi}{2} = f_H \quad \text{and} \quad \frac{R}{R \cos\phi} = f_v$$

as the horizontal and vertical foci. If we now allow ourselves to think of two different mirror radii in the two planes, we can solve these for $f_H = f_v$ —— or point focus.

$$\frac{R_H \cos\phi}{2} = \frac{R_v}{2 \cos\phi}$$

$$\Longrightarrow \cos^2\phi = \frac{R_v}{R_H}$$

7

This mirror is the toroidal mirror. Geometrically, the surface may be formed by rotating a circular arc of radius R_V about a second point which is farther away. See Fig. 3.

We can now solve for the R_V which will cause the horizontal and vertical foci to coincide. This is a tremendous increase in focal properties at $10°$ incidence, from about 1500 μ to 1 μ. As we approach a demagnification of 1 to 2 at around $45°$ incidence, however, the size of the image spot goes up to around 30 μ. This behavior supports the rule of thumb for toroidal mirrors which says that they should be used at no higher magnifications than 2 to 1. If we move the object closer to the mirror at the higher incidence angles, and hence move the magnification back to 1 to 1, the point focus returns. This is shown in the table in Fig. 3. In this case, the image and object distances were set equal: $i = 0$; and obtained from the condition for a horizontal focus.

$$\frac{1}{0} + \frac{1}{i} = \frac{1}{f_H} = \frac{2}{R_H \cos\phi} = \frac{2}{0}$$

$$\Longrightarrow 0 = R_H \cos\phi = i \text{ (by definition).}$$

This we can recognize as the representation of a circle expressed in polar form. This is an important fact for grating monochromators; spherical and toroidal reflection gratings form their spectra along this "Rowland" circle, named after the inventor of the concave reflection grating.

We have seen the limits to which our simple formulae may be pushed in describing focal properties of mirrors at very high angles. A hint for the explanation of the defocusing which the 5 cm x 5 cm toroid gave above $70°$ incidence may be seen by looking at the last entry in the table in Fig. 3. The size of the toroid was decreased in this case in the direction perpendicular to the plane of incidence. The defocusing drops from 120 μ to 6 μ. Remember the mirror's minor radius is now very short, $\sim$ 15.2 cm; and the 5 cm x 5 cm mirror subtends a large angle at this distance. In shortening the mirror to 5 x 1/cm, we have eliminated that portion of the toroid which deviates most from the ideal mirror shape which will focus our point object to an exact point. This shape is the ellipsoid. It has not been greatly used because of difficulty in manufacture. If you will recall the definition of the ellipse and ellipsoid, you will see that it can provide point to point focusing at magnifications other than 1 to 1. The sphere and the toroid perform well in those regions where they are a good approximation to it. At unity magnification and $0°$ incidence angle, the sphere gives an exact focus because it is a degenerate ellipsoid. Near unity magnification, the toroid provides a simple, effective substitute even at relatively

Fig. 3

The Toroidal Surface
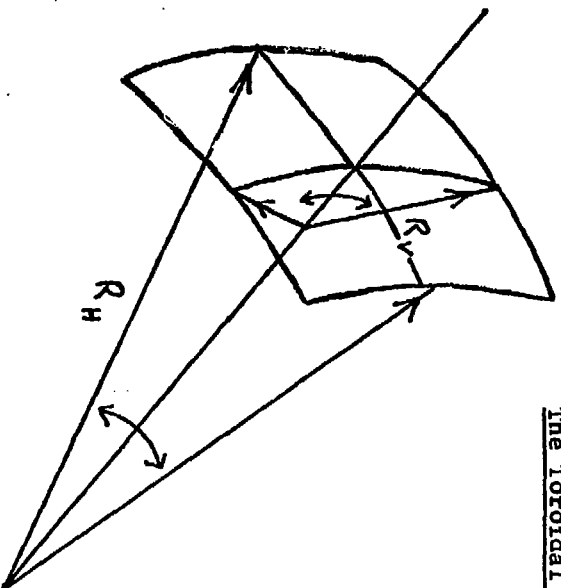
Major radius = 2000 cm
All distances in cm unless noted
* indicates 5 cm x 1 cm mirror, all other cases 5 cm x 5 cm

incidence angle	height of hor. focus in spherical case	distance to horizontal focus in spherical case	distance to vertical focus in spherical case	vertical radius for toroidal case	toroidal case spot dimension	magnification	toroidal case spot dimension m = 1	m = 1 image and object distance
10	0.149	1940	2062.7	1939.7	1 μ	0.97	<1 μ	1970
20	0.552	1772	2274.3	1766.0	6	0.89	<1	1879
30	1.103	1527	2732.1	1500.0	8	0.76	<1	1732
40	1.675	1242	3758.8	1173.6	22	0.62	<1	1532
50	2.163	947.2	7003.4	826.4	35	0.47	<1	1286
60	2.502	666.7	∞	500.0	71	0.33	1	1000
70	2.665	412.6	-6329.9	234.0	150	0.21	2	684
80	2.658	190.2	-3064.2	60.31			20	347.3
85	2.597	91.13	-2422.2	15.19			120	174.3
*85				15.19			6	174.3

high incidence angler.

Ray Tracing Mirrors and Gratings

Up to now, we have been investigating the limits of optical formulae using an exact ray trace. We now will describe it in some detail. Let us choose cartesian coordinates with the x axis perpendicular to the center of the mirror and the y axis to be in the horizontal or principle plane. The angle of incidence, α, will be chosen positive implying the angle of reflection, β, to be negative. Directions in space will be specified by direction numbers which are defined by $c\ell$, cm, and cn; where c is any constant and ℓ, m, and n are the cosines of the angles between the direction and the axes. For example, the x direction has direction numbers 1,0,0, or 2,0,0, or 3,0,0, etc.

Our object point will be given as (X_a, Y_a, Z_a) and mirror point will be given as (X_p, Y_p, Z_p). The direction cosine set for the incoming ray is:

$$\frac{X_a - X_p}{D}, \quad \frac{Y_a - Y_p}{D} \quad \frac{Z_a - Z_p}{D} \quad D = \left[(X_a - X_p)^2 + (Y_a - Y_p)^2 + (Z_a - Z_p)^2 \right]^{-\frac{1}{2}}.$$

A direction number set is then $(X_a - X_p)$, $(Y_a - Y_p)$, $(Z_a - Z_p)$. (X_a, Y_a, Z_a) is given by the problem at hand, as is α. Y_p and Z_p are known by the assumed size of the mirror. In the case of the sphere, one easily solvable quadratic equation gives X as a function of Y and Z.

$$(X-R)^2 + Y^2 + Z^2 = R^2$$

In the case of the toroid, however, the defining equation is not readily solvable for X.

$$0 = -X^2 - Y^2 - Z^2 + 2RX - 2R(R-\rho) + 2(R-\rho)\left[(R-X)^2 + Y^2\right]^{\frac{1}{2}}.$$

One may find X numerically to the degree of precision of a digital computer by Newton's method. This method iterates rapidly to an approximation for X_p good to eight decimal places, and uses the following formula:

$$X_{n+1} = X_n - \frac{f(X_n)}{f'(X_n)}$$

where $f(X) = 0$ is the defining equation for the toroid and

$$f'(X) = \frac{\delta F}{\delta X} = 2(R-X)\left[1 - \frac{R-\rho}{(R-X)^2 + Y^2 \,^{\frac{1}{2}}}\right].$$

10

Zero is used as the initial X_n.

We need now the normal to the surface at (X_p, Y_p, Z_p) in order to apply the law of reflection. The direction numbers of the normal to the optical surface are readily available from our defining functions:[6]

sphere $F_s(X,Y,Z) = 0$ $\ell_n = \dfrac{\delta F}{\delta X} = -(X_p - R)$

$m_n = \dfrac{\delta F}{\delta Y} = -Y_p$ $n_n = \dfrac{\delta F}{\delta Z} = -Z_p$

toroid $F_T(X,Y,Z) = 0$ $\ell_N = \dfrac{\delta F}{\delta X} =$ see above

$m_N = \dfrac{\delta F}{\delta Y} = 2Y_p \left[\dfrac{R-\rho}{\left((R-X_p)^2 + Y_p^2\right)^{\frac{1}{2}}} - 1 \right]$ $N_N = \dfrac{\delta F}{\delta Z} = -2Z_p$

We have enough information to find the direction of the outgoing reflected ray from point P. Let α' be the angle between in incoming ray and the normal to the mirror at P, and let β' be the angle between the outgoing ray and the normal.

We may write down from solid geometry,

$$\cos \alpha' = \frac{\ell_{ap} \ell_n + m_{ap} m_n + n_{ap} n_n}{D_{ap} \cdot D_n}$$

where $D_x \equiv \left[\ell_x^2 + m_x^2 + n_x^2 \right]^{\frac{1}{2}}$ and $\ell, m,$ and n are direction numbers,

and $\cos \beta = \dfrac{\ell_{pf} \ell_n + m_{pf} m_n + n_{pf} n_n}{D_{pf} \cdot D_n}$ (1)

where pf denotes the outgoing ray. By the law of reflection these three lines specified by the two rays and the normal all lie in a plane and $|\alpha'| = |\beta'|$. We can therefore write

$$\cos\left[|\alpha'| + |\beta'|\right] = \cos |2\beta'|$$
$$= \frac{\ell_{ap} \ell_{pf} + m_{ap} m_{pf} + n_{ap} n_{pf}}{D_{ap} \cdot D_{pf}} \qquad . \qquad (2)$$

Equations (1) and (2) provide us with two equations in the three unknown direction numbers ℓ_{pf}, m_{pf} and n_{pf}. We only need these two because the three direction numbers are not all independent. The cosine of the sum of two angles is expanded by the identity.

$$\cos (\alpha + \beta) = \cos\alpha \cos\beta - \sin\alpha \sin\beta$$

This can now be repeated for a grid of points on the mirror surface. In addition, since the object is usually not a point but a circular or rectangular aperture through which light is passing, a grid of object points must also be calculated. In general, then, we have k x ℓ sets of direction numbers where k and ℓ are the number of mirror and entrance aperture (slit) points, respectively.

In order to display this information in a usable form, we now take the outgoing principal ray from the center of the mirror, and choose the point along it which is of interest. This may be anywhere we wish, but is generally the point of horizontal or vertical focus. For example, we may find (X_f, Y_f, Z_f) the coordinates of this point from the reflection law and the condition for horizontal focus. The focal plane is then the plane perpendicular to the outgoing central ray at this point.

$$X_f(X-X_f) + Y_f(Y-Y_f) = 0$$

A spot diagram may be produced by finding the points of intersection of all of the lines defined by the k x ℓ direction number sets. Remembering that P denotes the mirror points, any point on any of the outgoing rays may be described by a single parameter λ where the coordinates are:

$$(X_p + \lambda\ell, \ Y_p + \lambda m, \ Z_p + \lambda n) \qquad .$$

If we put these values for X and Y into the equation for the focal plane, we may solve for λ and find the coordinates of intersection.

$$\lambda = \frac{X_f(X_f-X_p) + Y_f(Y_f-Y_p)}{\ell X_f + m Y_f}$$

We are now one step from plotting our spot diagram. We now must rotate our original coordinates around the Z axis so that the new X' axis is along the central outgoing ray. This will allow us to then plot the values Y' and Z' for our focal spot. X' will now be the same for all of the intersection points and will be equal to the distance along the central ray which we chose to observe the focal properties. The rotation is accomplished with the following matrix multiplication.

$$\begin{pmatrix} X' \\ Y' \\ Z' \end{pmatrix} = \begin{pmatrix} \cos\phi & \sin\phi & 0 \\ -\sin\phi & \cos\phi & 0 \\ 0 & 0 & 1 \end{pmatrix} \begin{pmatrix} X \\ Y \\ Z \end{pmatrix}$$

where ϕ is the angle of reflection (taken positive).

We have now covered the simpler case of ray tracing a mirror. For the case of the grating we will present the concepts that are necessary, but not treat them in such analytical detail. Let's look at the ruled grating case where grooves are equidistant along the chord of the circular arc. This is more precisely stated that the grooves are located by the intersection of a set of equally spaced parallel planes and the spherical or toroidal surface. The places are spaced a distance D_O apart and have equations:

$$Y = \pm nD_O \quad n = 0,1,2 \ldots$$

The law of reflection is replaced by the grating equation which allows $\alpha \neq \beta$;

$$\pm \frac{n\lambda}{D_O} = \sin\alpha + \sin\beta \quad \text{(a sign convention must be adhered to for } \alpha,\beta)$$.

The condition for horizontal focus (if we use it) must be generalized to:

$$\frac{\cos^2\alpha}{r} - \frac{\cos\alpha}{R} + \frac{\cos^2\beta}{r'} - \frac{\cos\beta}{R} = 0 \quad ,$$

where r and r' are the entrance and exit slit distances. This reduces to the previous for when $\alpha = \beta$.

The application of the grating equation becomes complicated at all points, except the center of the grating. Note that the grating grooves are <u>not</u> equally spaced on the mirror surface. This requires that D_O be adjusted by the following equation, producing an effective grating constant as a function of position on the grating.[7]

$$D = D_O \Big/ \left[1-(Y_p/R)^2 \right]^{-\frac{1}{2}}$$

This expression may be confirmed somewhat by visualizing what happens at $Y_p = R$ (a hemisphere for the spherical case). In addition, one must be quite careful about defining the α and β of the grating equation. The grating equation applies to cases where α and β are measured in a plane perpendicular to the grooves and containing the surface normal. This is, in general, not the same plane as the

plane of reflection. To ray trace properly, the grating equation becomes[7]

$$\pm \ \frac{n\lambda}{D} \ = \ (\sin\alpha' + \sin\beta') \ \cos\delta$$

where primes indicate that α' and β' are not necessarily the incidence angle and diffraction angle, either at the mirror center or at the point in question. δ is the angle between the plane of reflection and the plane defined above in which α' and β' are measured.

Application of the Ray Trace Program to a
Hypothetical Toroidal Grating Monochromator

The usual method of concave monochromator design follows the application of Fermat's Principle and the diffraction condition to the optical path function. The optical path is merely the geometrical path in this case because in a vacuum the index of refraction is unity. If F is the optical path from object point to grating point to the intersection with the gaussian image plane, the requirement that F be stationary with respect to displacements along the grooves requires (1), and the diffraction condition requires (2).*

$$(1) \ \ \frac{\partial F}{\partial Z} \ = \ 0 \qquad (2) \ \ \frac{\partial F}{\partial Y} \ = \ \frac{m\lambda}{d} \ \ m = 0,1,2 \ .....$$

F is expanded in a power series, and the different terms are associated with the various aberrations in the image. My colleague, Dr. Malcolm Howells of the National Synchrotron Light Source Staff, has provided me with the parameters of a hypothetical monochromator designed in this fashion.

Figure 4 shows the toroidal grazing incidence monochromator design. It is intended for the 5Å to 50Å region of the spectrum. The entrance and exit directions are fixed. The incidence and diffraction angles are varied by rotation of the grating around the Z axis. The $\Delta\lambda$'s were computed by adding the image blur from the various aberration terms in the following manner:

$$\Delta\lambda \ = \ \Delta\lambda_1 \ + \ \Delta\lambda_2 \ ..... \ \Delta\lambda_n \qquad \qquad ,$$

where n is the number of terms considered to be significant. In this case up to and including terms of 4th power in Y and Z. $\alpha + \beta = 174°$ was chosen to achieve high reflectivity at these short wavelengths. The toroidal shape and short height of the rulings conform to our previously covered ideas about grazing incidence focusing.

___

*This may equal zero, also depending on the definition of F.

Fig. 4 <u>Toroidal Grating Monochromator</u>
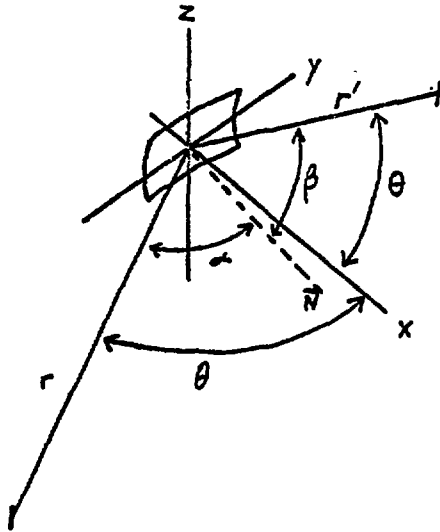
R = 20m
rho = 0.002716R
r = 0.05187R
r′ ≈ 0.04683R
2θ = 174°
grating height 1cm
grating width 5cm
300 grooves/mm

$\lambda(\overset{\circ}{A})$	$\Delta\lambda$ from optical path theory $\overset{\circ}{A}$	I width of exit spot from ray tr. μ	II dispersion in $\overset{\circ}{A}/\mu$	I x II $\overset{\circ}{A}$
5	0.158	81.3	0.00180	0.147
10	0.154	80.8	0.00175	0.142
20	0.188	111.5	0.00165	0.185
30	0.233	141.5	0.00155	0.220
40	0.356	231.2	0.00145	0.336
50	0.531	376.5	0.00135	0.509

The values in the table are for a point object.

In order to compare the $\Delta\lambda$'s from the aberration theory with the ray trace diagrams, we must calculate the dispersion of the monochromator.

For the central ray, the simpler grating equation holds:

$$\frac{m\lambda}{d} = \sin\alpha + \sin\beta \qquad .$$

Holding α constant and differentiating with respect to β, we obtain:

$$\frac{d\lambda}{d\beta} = \frac{d\cos\beta}{n} \qquad .$$

Now, in the usual physicist's manner of playing fast and loose with the calculus, we write where ℓ is the horizontal coordinate in the focal (exit slit) plane,

$$\frac{d\lambda}{d\ell} = \frac{d\lambda}{d\beta}\frac{d\beta}{d\ell} \text{ but } r'd\beta = d\ell \Rightarrow \frac{d\lambda}{d\ell} = \frac{d\lambda}{r'd\beta}$$

$$\frac{d\lambda}{d\ell} = \frac{d\cos\beta}{r'n} \qquad .$$

These values are tabulated in the figure and allow us to convert between $\Delta\lambda$ and distance in the focal plane.

Figure 5 shows the results of the ray trace for the 30Å case. The points are the intersections with the focal plane of the rays from a grid of points spaced around the edge and inside of the grating surface. As a first approximation we can take the total distance between extreme rays of 141.5 μ as the defocus. Multiplying this by 0.00155Å/μ, reciprocal linear dispersion gives 0.220Å of blur. At first glance, this compares well with the 0.233Å from the optical path theory. A better ray trace would be obtained by using a denser grid of grating points, and considering the density of dots in the image spot diagram. Most of the energy is likely in a smaller width than 141.5 μ. Figure 6 demonstrates the power of the ray trace method. Four object points were added at Z = ± 250 μ, ± 500 μ to evaluate the effects of a finite entrance image size. It is seen that the spot distribution changes as the object point moves out of the principal plane.

We plan to generalize our ray trace program in the future to include deviations from the ideal figure of the mirror surface. We also plan to include other cases, such as holographically recorded gratings, to supplement the straightforward approximation used here of treating the grating as a set of small plane gratings located at

Fig. 5 <u>Focal Plane Ray Trace Diagram for Single Object Point</u>
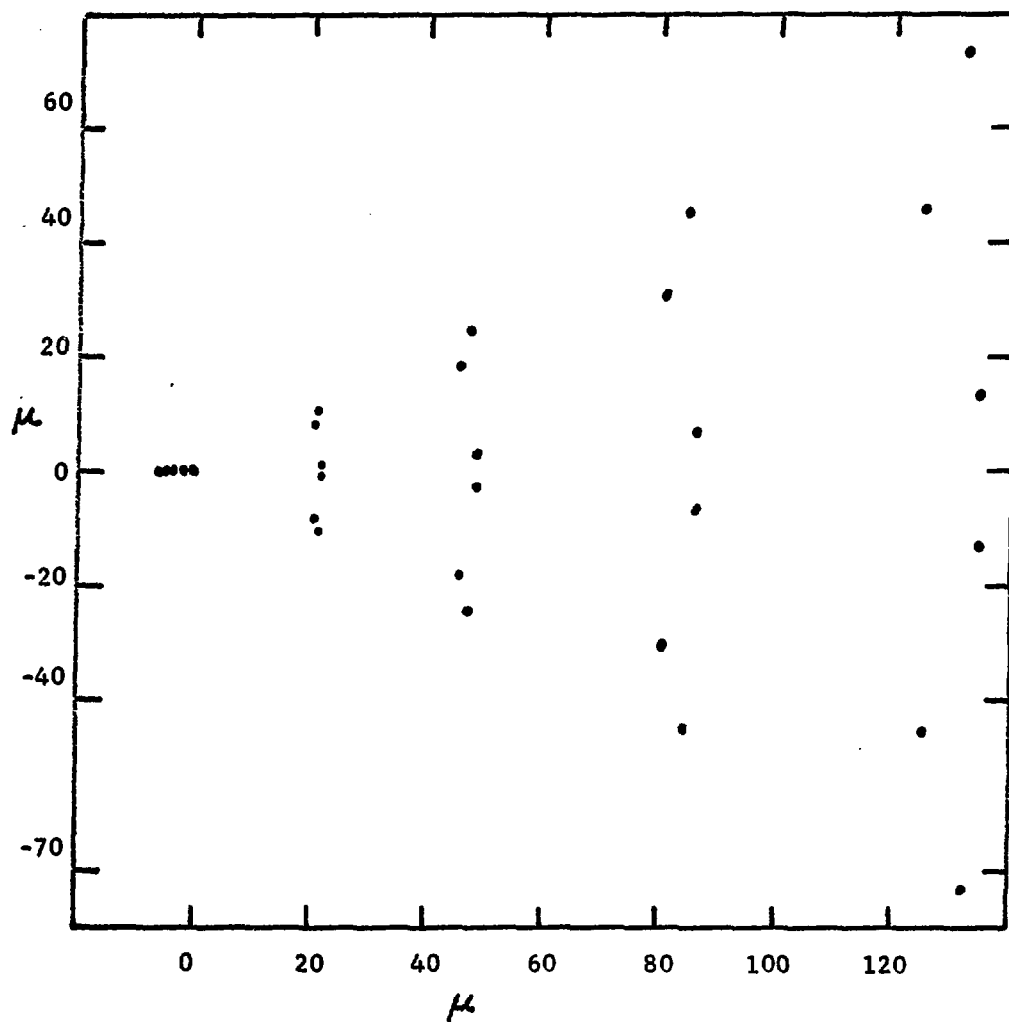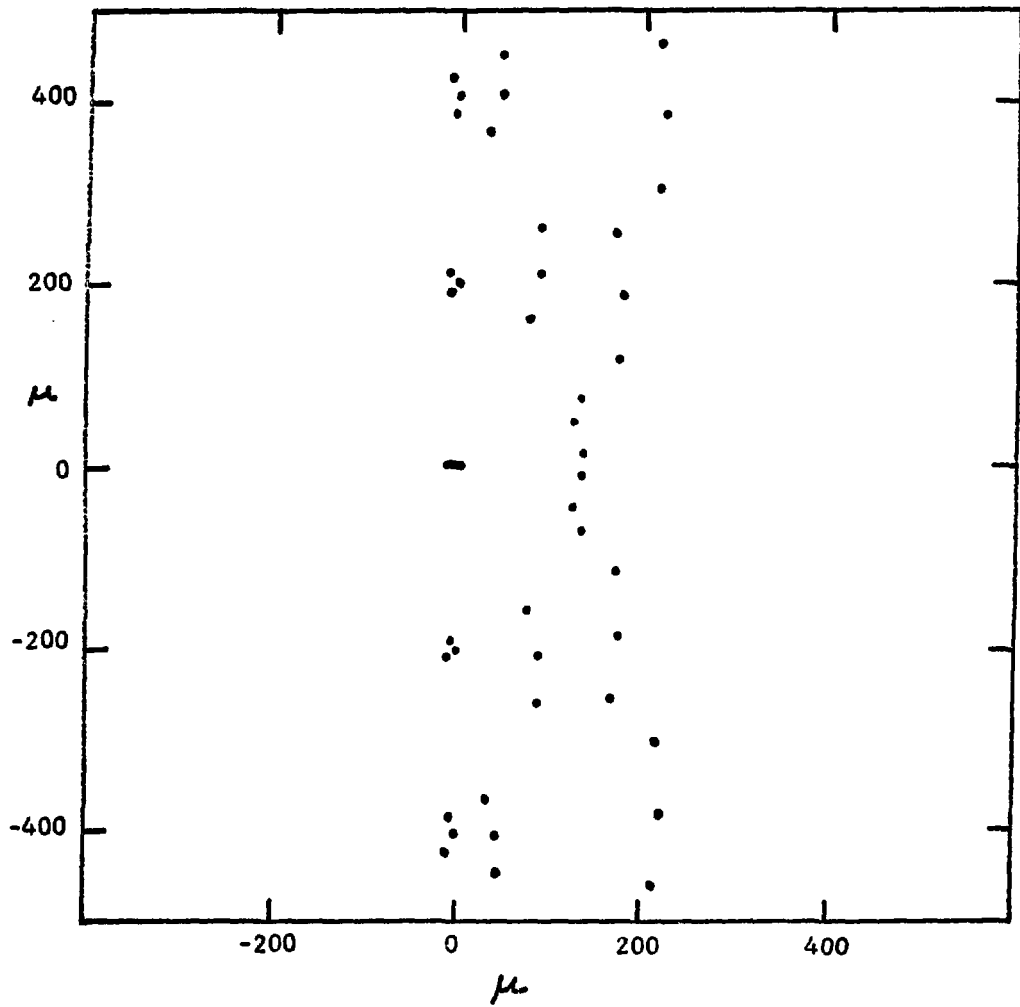
$\lambda = 30 \overset{o}{A}$

Fig. 6 Focal Plane Ray Trace Diagram for a Grid of Object Points

$\lambda = 30 \text{ Å}$

points at z = 0, $\pm$250, $\pm$500 μ

each mirror point.

Acknowledgements

References

1. Shirley, D. A., "Beam Line Chemistry", Workshop on X-ray Instrumentation for Synchrotron Radiation Research, SSRL Report No. 78/04, p. VII - 80, 1978.

2. Laurenson, L., "Perfluoropolyethers as Vacuum Pump Fluids", Research/Development, p. 61, November, 1977.

3. Rehn, V. and Jones, V. O., "VUV and Soft X-ray Mirrors for Synchrotron Radiation", SSRL Report No. 77/13, 1977.

4. Giles, J. W., McKinney, W. R., Freer, C. S., and Moos, H. W., "An Image Stabilized Telescope-Ten Channel Ultraviolet Spectrometer for Sounding Rocket Observations", Space Science Instrumentation, Vol. 1, No. 1, p. 51, 1975.

5. Blewett, J. P., ed., "Proposal for a National Synchrotron Light Source", BNL 50595, Vol. 1, 1977.

6. Widder, D. V., Advanced Calculus, 2nd Ed., Prentice Hall, Englewood Cliffs, N. J., p. 107, 1961.

7. Kastner, S. O. and Neupert, W. M., "Image Construction for Concave Gratings at Grazing Incidence by Ray Tracing", JOSA, Vol. 53, No. 10, pp. 1180-1184, 1963.

General References

Techniques of Vacuum Ultraviolet Spectroscopy, James A. R. Sampson, John Wiley & Sons, Inc., New York, 1967.

Vacuum Ultraviolet Spectroscopy, A. N. Zaidel' and E. Ya Schreider, Halsten Press, New York, 1970.